Receiving Editor: T. FREUND
Cytology, Cellular and System Neuroscience
Institute of Experimental Medicine, Hungarian Academy of Sciences, Szigony u. 43, Budapest 8, H-1083, Hungary.

Intra-cortical complexities revealed in the primary somatosensory cortex of rats

Zi-Hao Wang[c], Ming-Hua Chang[a], Jenq-Wei Yang[a], Jyh-Jang Sun[a], H.C. Lee[b] and
Bai-Chuang Shyu[a,*].

[a]Institute of Biomedical Sciences, Academia Sinica, Taipei, 11529, [b]Department of Physics and Institute of Biophysics, National Central University, Chungli, 320, Taiwan, ROC and [c]Institute for Neuroinformatics, UNIZH / ETHZ, Zurich, 8057, Switzerland

Running title: Complexities in primary somatosensory cortex

Total number of pages: 49
Figures: 7
tables: 5

Total number of words in: (i) the whole manuscript; 5731
(ii) the Abstract; 233
(iii) the Introduction; 775

***Corresponding author:**
Bai-Chuang Shyu,
Institute of Biomedical Sciences,
Academia Sinica,
Taipei, 11529,
Taiwan, ROC
phone:: 886-2-2652-3915
Fax no: 886-2-2782-9224
Email: bmbai@ccvax.sinica.edu.tw

Key words: Cortical layers; correlation dimension; fractal exponent; nonlinear dynamics; power spectrum

Abstract

Correlation dimension can give a good measure of complexity underlying the system. It is still not clear the system complexity embedding in different cortical layers that processed the neuronal information flow in vertically organized column. The aim of present study was to estimate the system complexity across different cortical layers by analyzing intracortical EEG signals using nonlinear analytical method and to identify the changes of layer-related complexity in different brain state. Male Sprague-Dawley rats were anesthetized under l % halothane. Sixteen channels of evoked or spontaneous EEG signals were recorded simultaneously across the six cortical layers in the somatosenseroy cortex with a single Michigan probe. The system complexity was assessed by computing correlation dimension based on the data analysis program of the Nonlinear Time Series Analysis. Cortical layer IV exhibited the largest correlation dimension value, 3.24, and that was significantly higher than other cortical layers. The correlation dimension in layers IV and II/III was significantly reduced after reversible deactivation of ventrobasal thalamic nucleus. The correlation dimension decreases while increasing halothane concentration from 0.75% to 2.0% and the percent decrease of the correlation dimension is highest in layer IV. The present findings suggest that the cortical layer IV maintains a higher complexity than that in the other layers and the complexity of mid-cortical layers was

subject to regulation from specific thalamic inputs and more sensitive to the changes in general state of brain excitation.

Introduction

Nonlinearity has been found to be embedded in brain dynamic processes from activities at the microscopic cellular level to macroscopic sets of connections at the cortical level (Babloyantz and Destexhe 1986; Theiler 1995). As a result the quantitative analysis of electroencephalogram (EEG) data by nonlinear dynamical methods has often been used to elucidate the underlying dynamics of neuronal processes. The scalar EEG time series in high dimensional Euclidean space can be reconstructed by the nonlinear time series analysis method (NTSA) (Kantz and Schreiber, 1997). With the help of the embedding theory (Takens, 1981), NTSA can be used to extract from EEG data quantities such as the largest Lyapunov exponent and correlation dimension (D_2) which have been used to quantify brain electrical activity (Jeong et al., 1998; Roschke et al.; 1994, Pereda et al., 1999; Kotini and Anninos, 2002). Correlation dimension is one of the characteristic invariants of nonlinear dynamics that can give a good measure of complexity of the underlying attractor in a dynamical system (Anokhin et al., 1996). Such dimensional complexity can be used to quantitatively characterize EEG signals: the greater the dimensionality, the more complex the signals. That is, by reflecting the complexity of neurophysiological processes generating the EEG signals, correlation dimension reveals the specificity of different brain activation states.

In the past few decades the NTSA technique has resulted in many successful prescriptions or predictions of brain states: physiological (Babloyantz and Salazar, 1985) or pathological brain states such as in epileptic seizure (Lehnertz et al., 1998; Van den Heyden et al., 1999; Ferri et al., 2001); Parkinson disease (Stam et al., 1995); Alzhheimer's (Jeong et al., 1998; Van Cappellen van Walsum et al., 2003); schizophrenia (Lee et al., 2001). Most of the EEG data used for analyzing in the non-linearity studies were recorded on the scalp or the cortical surface. Intra-cortical deep EEG analyzed using non-linear method was also reported (van der Heyden et al., 1999), in which no comparison of complexities in different cortical layers was made. Cytoarchtectual studies have shown that the neocortex consists of six distinct layers parallel to the cortical surface. In the vertical dimension, neurons are organized into groups linked synaptically across the horizontal layers. The vertically oriented narrow chain of neurons, called the minicolumn, is regarded as the basic unit of the neocortex (Mountcastle, 1997). Minicolumns are further connected by short-range horizontal connections and organized into functional modules of a higher order called cortical columns which are formed by neurons having similar sets of physiological properties (Powell and Mountcastle, 1959). This modular organization is a widely recognized principle of design for structure and function of the brain (Jones, 2000; Mountcatcastle, 2003; Szentagothai, 1975). The cortical column is a complex

processing and distributing unit that links a number of inputs to a number of outputs via overlapping internal processing chains. All neurons inside the column are tightly connected and the neuronal connections extend to adjacent columns and columns far across the cortex and into subcortical areas, particularly the thalamus. Cortical layer IV receives the major inputs from the thalamus and transmits signals to the supragranular and infragranular parts of the column. The thalamus receives sensory information from peripherals and all parts of the cortex and works together with the cerebral cortex to create a feedback circuit by passing information from the infragranular cells of the cortex to the thalamus and then back to the layer IV cells of the cortex (Scannell et. Al. 1999). The reciprocal connections within cortico-thalamo-cortical systems were proposed to underlie gate/gain mechanisms at the early stage of sensory information processing (Crick and Koch 1998). It is still not clear what are the relative changes of the system complexity in the neuronal information flow that are processed in this basic cortical module. Thus we hypothesized that system complexity may differ in different cortical layers and that the complexity in different cortical layers may be subject to change in general excitatory states and more specifically to the thalamic input drives. The aim of present study is to investigate the complexity changes across different cortical layers in the primary somatosensory cortex of rats and the factors that may influence the cortical

layer dependent complexity. EEGs from cortical layers I to VI were simultaneously recorded and analyzed with NTSA method. The averaged correlation dimension and scaling exponent in double log scale spectrum of each layer were recorded to elucidate the neuronal activities within cortical columns. The changes of intra-cortical complexity in different brain states were evaluated by varying anesthesia levels. The influences of the specific thalamic inputs on the system complexity were investigated by studying the effect of reversibly deactivating the ventral posterior lateral (VPL) thalamic nucleus.

Methods and materials

Experimental animals

Male Sprague-Dawley rats (National Laboratory Animal Center, Taipei, Taiwan, ROC) of 250-350g weighted were used. Rats were housed with artificial light systems, 12hrs light/dark. The room temperature is 22℃ and rats are free access to food and water. All experiments were carried out in accordance with the National Institutes Guide for the Care and Use of Laboratory Animals, and approved by, the Academia Sinica Institutional Animal Care and Utilization Committee. All efforts were made to minimize animal sufferings and to use a minimal number of animals.

Animal preparation

Rats were initially anesthetized with halothane (2-3 % in 30%/70% nitrous

oxide/oxygen mixture) during surgical operation. Rectal temperature was measured and maintained at least 36.5℃ via a homeothermo blanket system (Harvard apparatus, USA). A PE-240 tube was inserted into the tracheal via tracheotomy and the rats can voluntarily inhale the halothane and oxygen mixed gas. The electrocardiogram was recorded on an oscilloscope. CO_2 concentration was monitored (Normpcap 200 oxy, Detax Instrumentarium Corp., Finland) and maintained within the range of 3-4%. Concentrations of inhaled halothane (0-2 minimum alveolar concentration) were monitored continuously using a calibrated infrared gas analyzer (Capnomac Ultima, Datex Ohmeda, Helsinki, Finland). Rat's skull was exposed and holes were drilled to allow electrodes access to the left primary somatosenseroy cortex or thalamic nucleus. Electric stimulation was given by passing a 0.1 ms, 1 mA square wave constant current from a pulse generator (Model 2100, A-M Systems, Inc., USA) on two stainless steel wires attached to the right hind paw.

Recording and data acquisition

Surface cortical field potentials evoked by electrical stimulation were firstly recorded by a tungsten electrode and systemically mapped on the hind limb projection area in the primary somatosensory cortex. A 16-channel (1x16) Michigan probe was then positioned to the recording site where the largest amplitude of the evoked field potential was previously obtained. The inter distance between each contact lead on the

probe was 150 μm. The recording depth covered from cortical surface to 2250 μm deep. Thus evoked or spontaneous EEG signals of different cortical layers (from cortical layer I to VI) were simultaneously monitored. One Ag-AgCl reference electrode was placed beneath the scalp. The data were acquired from an integrated 16-channel Medusa Digital BioAmp amplifier and DSP data acquisition system based on PC system (TDT Inc., USA).

Reversible deactivation of VPL thalamic nucleus

The location of the left VPL thalamic nucleus was functionally identified by recording the thalamic responses to electrical stimulation of the right hind paw. A handmade hybrid electrode which combines recording tungsten electrode and microinjection micro-tube (20 μm ID, 90 μm OD, MicroFil, WPI Inc., USA) was constructed. The micro-tube was filled with 2% lidocaine (Xylocaine, AstraZeneca, Sweden) and connected with a perfusion pump. This recording-microinjection electrode was inserted with an angle of insertion of about 40 degree to the right cortex and consequently penetrated into the left VPL thalamic nucleus. The point of insertion is at coordinate 3.0 mm posterior to bregma and 2.0 mm lateral to the bregma in the right side. The thalamic activities were monitored and searched while the recording electrode was advanced and electrical stimulation is continually applied to the right hind paw. The electrode was fixed at the location where the short latency thalamic

unit responses were recorded. To deactivate the thalamic responses, 1 μl of 2% lidocaine was infused for two min into the VPL thalamic nucleus. The inhibitory effect of the lidocaine and the recovery on the thalamic responses to the electrical stimulation was monitored continuously.

Alteration of the general brain state in variant halothane concentration

Three concentrations 0.75%, 1% and 2% were employed to establish the general background activities. In each concentration of the halothane, concentrations of inhaled halothane (0-2 minimum alveolar concentration) were monitored continuously using a calibrated infrared gas analyzer. At least 5 min was allowed after changing of concentration to maintain in the stable condition before the multichannel EEG signals were recorded. The heart rat and reflex activity were monitored and tested periodically during the recording session.

Current Source density (CSD)

The electrical stimulated evoked field potential was recorded for 1s (6000points) on a single trial. Twenty trials of evoked field potentials were averaged for each channel. To accurately locate the synaptic currents that mediate the local extracellular potentials, the 16 channels of averaged field potentials were subjected to one-dimensional, three-point CSD analysis formula (Freeman and Nicholson, 1975; Mitzdorf, 1985). The CSD of channel n, I_n, was derived from the second spatial

derivations of the averaged field potentials, ϕ

$$I_n = -\left(1/4h^2\right)*\left(\phi(x-2h) - 2\phi(x) + \phi(x+2h)\right)$$

Where h = 150 μm is the inter distance between channels, and x is the coordinate of each channel. The spatial profiles of current sinks and sources along the axis of the electrode were evaluated. The averaged 10 ms data before stimulation was chosen as baseline. The current density value less than the baseline value is designated as sink current, assuming the inward directed current. Value larger than the baseline is designated as source current.

Nonlinear analysis

The data analysis program was based on the Nonlinear Time Series Analysis (TISEAN) sub programs (in C language) written by Hegger et al. (1999). The main program was constructed in MATLB. Each epoch of 8 s (sampling rate 250 Hz; 2000 points) spontaneous EEG data was used for data analysis. Takens's delay embedding theorem (1981) was used to reconstruct the phase space of an attractor. Phase portraits are constructed by expanding a single scalar time series $\{x_1,...,x_i,...,x_N\}$ into m-dimensional vectors

$$\vec{X}_i(t) = \left(x_i, x_{i-n_\tau}, x_{i-2n_\tau},..., x_{i-(m-1)n_\tau}\right)$$

where $i = N,...,1+(m-1)\tau$ and τ denotes the time lag. The first local minimum of mutual information of the scalar time series estimated the time lag τ and

the false nearest neighbor method was used to determine the minimal sufficient embedding dimension *m*. In our data, *m* was around 4~6, and τ was about 80 ms. The D_2 was estimated by using the Grassberger & Procaccia's (1983) algorithm. The correlation sum of a given attractor in phase space is defined as

$$C(r)=\frac{2}{(N-W)(N-W-1)}\sum_{i=1}^{N}\sum_{j=i+1+W}^{N}\Theta\left(r-\left\|\vec{\mathrm{X}}_i-\vec{\mathrm{X}}_j\right\|\right)$$

where Θ is the Heaviside step function and W is the Theiler (1986) window. Since $C(r)\propto r^{D_2}$, the linear slope of $\log C(r)$ versus $\log r$ plot gives the estimated D_2 for the scaling region. The D_2 obtained by averaging 15 subsets among each 120 s recording of each channel represented the dimensional complexity of each channel in different cortical layers.

Surrogate data analysis

In the present study nonlinear analysis tool was used to obtain the correlation dimension as the indicator to the dimensional complexity of the EEG signals. However, it had been reported that for nonlinear algorithms can mistake linear correlations for determinism in time series data (Nicolis and Nicolis, 1984a; Grassberger, 1986; Nicolis and Nicolis, 1984b; Grassberger, 1987), in particular those of the power law type (Osborne and Provenzale, 1989; Theiler, 1991). Thus the test of the nonlinearity hidden in the EEG signals becomes important before the application of the nonlinear methods on the analysis of data. The idea is to test results against the

null hypothesis of a specific class of linear random processes, e.g. the Gaussian linear stochastic process. One of the most popular of such tests is the method of "surrogate data" (Schreiber and Schmitz, 1996), which can be used with any nonlinear statistic that characterizes a time series by a single number. In the present investigation the surrogate data and its corresponding values of correlation dimension are both obtained from the original EEG signals using the TISEAN (Schreiber and Schmitz, 1996)

Power spectrum analysis

The power spectrum density computed from Fast Fourier Transform of different frequency bands was also analyzed. It included low frequency (1~8Hz), alpha (8~12.5Hz), Beta (12~30Hz), and Gamma (40~70Hz) bands. The scaling exponent, β was obtained from linear regression fit of log-log power spectrum plot within frequency range 2~70 Hz.

Statistics

The test of non-linearity was carried out by Wilcoxon matched-pairs signed-rank test comparing pairs of D_2 values calculated on the original data sets and their corresponding surrogate data sets. The D_2 and scaling exponent in different cortical layers and different groups were compared using ANOVA. Two-way ANOVA was used to analyze the effects of different halothane concentrations and thalamic deactivation on the D_2 in different cortical layers. Tukey test was used for the statistic

scheme for post hoc test between different subgroups.

Experimental procedure

Once the rats were fully prepared, evoked field potential by electrical stimulation of contralateral hind paw were recorded and the CSD method was applied to characterize the current source and sink along different channel channels. Secondly, the spontaneous EEG signals with 250 Hz sampling rate were recorded for 160 seconds. Both linear and nonlinear time series analysis methods were applied. Thirdly, the level of anesthesia was changed with adjusting concentration of halothane varied from 0.75%, 1% to 2%. The same recording process was repeated before and after the concentration changes. Finally, in four rats, the effect of the thalamic deactivation was investigated and the multichannel EEG signals were sampled before, immediately and 30 min after the injection of 2% lidocaine into the functionally identified VPL thalamic nucleus.

Histology

In order to verify the corresponding cortical layers in each recording points, in the end of the experiment a small lesion was made by passing a DC anodal current (30 μA for 30s) to the 16^{th} contact lead, the deepest electrode, on the probe. Another lesion was made at the same lead after the Michigan probe withdrawal for 1000 μ m. In experiment of selective thalamic deactivation, the recording-microinjection hybrid

electrode was withdrawal from the brain and then replaces the lidocaine in the micro tube with pontamine sky blue (Sigma, USA, 2% dissolved in 0.9% saline). After re-insertion the hybrid electrode into the same VPL site, 1 μl of sky blue was infused into the VPL to mark the injection site and for estimation of the approximate diffusion area of lidocaine. The brains were cut in 60 μm thick coronal sections using cryostat and the sections were stained with cresyl violet (Sigma, USA). Drawings were made in sections with clear electrode tracks and lesion marks. The cortical layers were identified by inspecting the shapes of neuron cells under microscope. The rat atlas of Swanson (1992) was used as reference when detail histological structures were estimated.

Results

To evaluate the system nonlinearity, 9 sets of multichannel EEG signals in resting condition from different rats were obtained. Mean and S.D. of D_2 from each channel of original and corresponding surrogate data were calculated from the TISEAN (Table 1). Significant difference was found between these two groups with paired t-test ($P< 0.001$).

Spontaneously activated complex brain activities in the primary somatosensory cortex as revealed by multichannel EEG recordings were observed among different recording channels. An example of 8 s epoch of simultaneous EEG time series

recordings in 16 channels was shown in Figure 1. Similar oscillatory waves but varied frequency, amplitude, phase and polarity of the EEG patterns across different channels were observed. Oscillation with fast frequency was noted in some segments of EEG recordings. From the histological verification of the corresponded recording channels, the approximate cortical layers distribution of each recording channel was labeled in the right side of the panel. The spontaneous EEG in superficial layers (I and II/III) exhibited many biphasic (positive/negative) potentials. These potentials tend to change their polarity from layer IV down to deeper layers. The CSD profiles of evoke field potential in one typical example were displayed in Figure 2. The latency of the earliest sink current in layer IV was about 15 ms following electric stimuli. Sink currents with longer latencies were distributed in superficial and deep layers. It appeared that activated synaptic events started from the layer IV and then flew upwardly to layer II & III and downwardly toward layer V & VI.

The EEG in 16 channels revealed low complexity with the averaged correlation dimension, D_2, ranged from 2.23 to 3.65 in five animals. One typical example of D_2 changed in different recording channels was shown in Figure 3a. D_2 was maximal in the recording channel 5. The correlation dimension D_2 quantified the geometrical complexity in the phase portrait. The delay phase diagrams measured from channels representing the different cortical layers are illustrated in Figure 3b. The topological

patterns are apparently different among channels. The channel number that corresponded to the same cortical layers in different animals were adjusted and grouped together. D_2 calculated from the channels contained in the same cortical layer were averaged and analyzed. The relationship between cortical layers and D_2 was obtained and shown in Figure 3c. Cortical layer IV exhibits the largest D_2 value (3.24 ± 0.03, mean ± S.E., n=5), which implied the most complex dynamical portrait in phase space. ANOVA and post hoc test showed that the D_2 of the layer IV is significantly different from all the other layers. The D_2 values of layer II/III and layer V are similar. The D_2 value of the cortical layer VI is significantly different from all the other layer except layer 1 (Table 2).

The power spectrums in linear scale of channels representing different cortical layers and typical examples are demonstrated in figure 4a-e. The differences of spectrum distribution among layers were observed. The averaged power spectrum densities (in figure 4 g) of low frequency, alpha, beta, and gamma bands in each cortical layer were calculated to illustrate the distinctions among layers. The low frequency component decreased dramatically in layer IV. In contrast, components of beta and gamma bands of cortical layer IV increased. The power spectrum in log-log scale also showed the scaling nature of the EEG. The spectra range of 2~70 Hz presented the power law $1/f^{-\beta}$ dependence. An example as shown in Figure 4 f, was

taken from channel 5 representing layer VI. The scaling exponent β was obtained from linear regression fit within range 2~70 Hz. The fitted slope on cortical layer IV is the lowest (0.95 ± 0.05) with respect to other layers. The EEG of cortical layer IV revealed more low amplitude and higher frequency fluctuation. The decreasing in low frequency component but increasing in high frequency part in the layer IV (Figure 4 g) makes the scaling exponent β small in this layer. Statistical evaluation showed that the β of layer IV is significantly different from all the other layers (Table 2).

In addition, the D_2 and β obtained from the same data set and in five different animals were compared and a negative linear correlation between D_2 and β was found and the correlation coefficient is 0.73 (n=5) (Figure 5).

The rats were treated in three different halothane concentrations 0.75%, 1% and 2%. The physiological effect of the anesthetic level was demonstrated by showing their influence on the profiles of the electrically-evoked sink source currents (Figure 6a). The amplitudes of the earliest sink in layer IV were -20.33 ± -7.62, -15.84 ± -4.19 and -12.54 ± -3.12 mV/mm^2 in 0.75%, 1% and 2% halothane concentration respectively. The peak latency of the evoked sink current was significantly lengthened when compared the values obtained between 2% and 0.75% halothane concentration (17.27 ± 0.67 versus 15.89 ± 0.54 ms). The D_2 was measured from the spontaneously EEG in 16 channels under different halothane concentration. The D_2 decreased

monotonically with increasing depth of anesthesia. In addition, there is tendency that D_2 not only decreased with increasing anesthesia depth but also with maximum D_2 shift to superficial channels (Figure 6b). The D_2 of each channel under 0.75% was treated as control values. The percent change of D_2 was calculated by divided the 1% or 2% D_2 in each channel with that of control values. The channel values attributed to different cortical layers were grouped and a result was shown in Figure 6c. The decreasing percentage of D_2 in layer IV, while halothane concentration is more than 1%, is larger than others. That is, layer IV is more sensitive to the change of anesthesia stage (Table 3).

The effects of different concentrations of halothane across cortical layers were examined. The data were analyzed by a 2-way repeated measure ANOVA with concentration and cortical layer as the within-subject variables (Table 4). The results showed that the D_2 were significantly different across each cortical layers, as indicated by a significant cortical layer main effect ($F(4, 49) = 4.71$, $p < 0.02$). Moreover, there was a 2-way interaction between concentration and cortical layer ($F(4, 49) = 11.70$, $p < 0.001$). Post-hoc tests showed that the higher concentration of halothane significantly depressed the activities of layer IV, V, and VI (all $p_s < .001$) but not of layer I and II/III. The complexity of the layer IV was suppressed to 24.6 % compared with the reduction of 7.5 % of that in layer I when halothane increased from

0.75 % to 2%.

To test the importantance of the thalamic input drive on the complexity as estimated from the spontaneous EEG signals, reversible deactivation of the thalamic VPL nucleus was performed. The experimental set up was shown in Figure 7, a. The hybrid electrode was advanced obliquely into the thalamic nucleus from the opposite side. The accurate location was identified by observing the excitation of the VPL thalamic unit activities by peripheral electrical stimulation, Figure 7, b, upper sweeps. Simultaneous multicannel EEG recording and the evoked CSD activation profiles of one typical example were plotted in Figure 7, b. The deactivation of both thalamic cortical responses was apparent after microinhection of 1 μl oflidocaine into the VPL thalamic nucleus (Figure 7, b). Thirty min after the lidocaine injection, both of the thalamic and cortical evoked activities recovered. The extents of the diffusion of lidocaine were delineated as the solid curves in 4 of test animals. The blackened area depicted the converging of the 4 overlapped diffusion areas and covered the most of the VPL thalamic nucleus. The D_2 data set were calculated from the spontaneous EEG signals obtained before, during and 30 min after the injection of lidocaine, and were plotted against the cortical layers (Figure 7 c). Two-way ANOVA showed that there were significant differences in layers and treatment conditions ($F(4, 39)=49.61$, $p<0.001$ and $F(2, 39)= 5.01$, $p< 0.05$ respectively, Table 5). Post-hoc tests showed that

there were significant differences in treatment conditions within layer IV (control v.s. lidocaine treatment, p=0.017 and lidocaine treatment v.s. recovery, p=0.001). There was a tendency of reduction of the D_2 in layer II/III after lidocaine treatment. However, the difference of lidocaine versus control groups was not statistically different.

Discussion

In the present study, the evaluation of the surrogate data provides strong evidence that the nonlinearity is a significant feature of the primary somatosensory cortex where the underlying deterministic interaction loops are likely to be revealed by examining their intra-cortical complexities using the nonlinear methods. Our results demonstrated that activities across the cortical layers showed different values of D_2. From the sink source current profiles evoked by electrical stimulation and combining with histological examination, the respective cortical layers can be accurately located. The value D_2 of cortical layer IV is the largest, followed by layers II/III, V, and I and finally VI. Cortical layer-dependent complexity can be expressed by D_2 and scaling exponent and these two values are reversibly related. The D_2 of layer IV was reduced significantly by temporally deactivation of thalamic VPL thalamic nucleus and the effect was reversible as indicated by the recovery of the thalamic and cortical evoked responses. The complexity changes in different cortical

layers were also subject to the changes of activity level regulated by halothane anesthesia.

Neurons in rodent primary somatosensory cortex receiving projections from mystacial vibrissae are organized in hollow, vertically oriented barrel (Woolsey and van der Loos, 1970). The cortical recording sites in the present study were in the area that receives thalamic afferents relayed inputs from the hind limb. The structure basis of the cortical module in this part of the primary somatosensory cortex was also found recently (Skoglund et al., 2004). Well-defined bundles of apical dendrites emanating from pyramidal cells were observed in this cortical region. The number of bundles consisting ascending apical dendrites through layer IV was estimated about 190 bundles/mm^2 and the average number of neurons that each bundle derived was estimated about 600 (Skoglund et al., 2004). Their distinct organization of neurons and dendritic bundles in rodent primary somatosensory cortex provide the anatomical basis for cortical cell modules. The common inputs, close contacts within the bundles and reciprocal connections both via intra-areal lateral connections and inter-areal feedback/feedforward pathways make these modules work synchronously and distributed to and coordinated widely separate cortical and subcortical areas. The D_2 calculation in the present study was based on the ongoing intracortical EEG activities under the anesthetized state. Spontaneous brain oscillations are associated with

neuronal excitability changes due to rhythmic spike trains fired by corticothalamic networks during sleep and waking (Steriade, 2003). Thus a very large part of the recorded intracortical EEG signals in a vertical column is most likely generated and maintained by the rhythmic thalamocortical loops and the reverberated activities in the input/output circuitries consisted in the cortical modules.

It is know that D_2s are proportional to the number of independent components containing in the total system (Egolf and Greenside, 1994). And it was found that systems with mixed feedback (both positive and negative feedback) and multiple feedback with different time constants are sources of chaos (Glass et al., 1987). Thus the finding of cortical layer-dependent complexity suggested that there is a differential distribution of the number of independent circuit components in each cortical layer. The high dynamical complexity indicated that more independent circuit components were comprised in the layer VI. The spiny stellate neurons in layers VI are the principle target of the thalamocortical axons as well as recurrent excitatory connection from other cell in the same layer (Peters and Kara, 1985a, 1987; Martin, 2002). This recurrent excitatory circuitry is controlled by both feedforward and feedback inhibition, which are mediated by distinct classes of inhibitory GABAergic interneurons (Kawaguchi and Kubota, 1997; Peters and Kara, 1985b). In highly recurrent layer IV network, the stabilization of neuronal network activities may be

achieved through a coordinated set of changes in excitatory and inhibitory circuitry. The strength of recurrent excitatory and feedback inhibition can be modulated by the thalamic input drives and in turn the modulated changes in layer IV excitability in response to thalamic inputs may enhance the ability of layer IV to amplify the input signals it receive (Feldmeyer et al., 2002; Stoop et al., 2002; Maffei et al, 2004). The importance of thalamic input drives to sustain the system complexity was substantiated by the present result of thalamic deactivation and the sensitivity of the layer IV to the general reduction of cortical activity. In our experiment the D_2 reduction in the cortex after lidocaine deactivation of thalamus recovered back to control level that coincided with the recovery of the thalamic and cortical evoked responses. Thus the observed changes of complexity are very likely a causal link of specific thalamic input activation rather than a plastic changes resulted from non-specific massive inhibition. Recent electrophysiological study indicated that neuronal circuit layer IV plays an important role on homeostatically regulate the intrinsic neuronal excitability and synaptic strength (Turrigiano and Nelson, 2004). The characteristic of the neuronal circuit in layer IV seems to fit the requirement for a nonlinear dynamic system and that is the property to meet the very rapid environmental change demand and is sensitive to the very weak initial condition that lead to wide spread changes by way of the output connections (Elbert et al., 1994).

The changes of D_2 across the different cortical layers could be attributed to change in a number of these independent circuit components reflected in the collective extra-cellular field potential and recorded by the electrodes in respective layers. From our CSD analysis of the cortical sink source patterns activated by the peripheral inputs, we found that the earliest sink occurred in layer IV and then the currents sweep upward to the layer II & III and downward to layer V and VI. This finding is in corroboration of current notion of the basic neuronal circuit and that is the intracolumnar processing leading to different output channels and cortical efferent neurons with different extrinsic targets are partially segregated; those of layers II/III project to other cortical areas, those of layers V/VI to subcortical structures (Douglas and Martin, 2004; Mountcastle, 1997). Each of the cortical layers have clear differences in synaptic organization and function that represent different processing stages. Different types of thalamic inputs terminate at different cortical depth with differences in arbor size and functional properties. Cortical layers which receive intercolumar relays from different thalamic recipient layers, have clear differences in physiological properties. Efferent projection neurons within different layers connect extrinsically to different regions of associate cortex or subcortical regions. Lateral connections in each layer join together tangentially very different extents of territory across the layers. Thus it may assume that the collective neuronal activities emerges

from an ensemble of independently active assemblies in the layer IV and transfers the information flow to more superficial or deeper layers. Consequently it causes more independently operating components to synchronize into the correlated activities, thus reducing the number of independent, autonomous components yielding a decrease of D_2.

Recent report using fractal analysis of neuronal 3D structures found that axons of neurons in primary visual cortex had similar complexity and were topographically self-similar (Binzegger et al., 2004). It will be interest to further investigate to see whether the difference in the distribution of the structure complexity in different cortical layers correspond to the different dimensional complexity in different cortical layers observed in the present study.

In the linear analysis, the EEG spectrum of layer IV showed a wider distribution. Thus the lower fractal exponent was obtained. Unlike the simple harmonics with identical peaks in frequency domain, the EEG presented the power law spectrum distribution which is usually observed in nonlinear systems. The higher dynamical complexity in phase space accompanies with the broader spectra distribution in the frequency domain. In the context of complexity analysis, D_2 is the average fractal measure in the reconstructed phase space where the trajectories of the phase portrait gives a distribution of the momentum for the dynamical system. Meanwhile β is the

scaling exponent that measures the momentum distribution as a function of the power spectrum densities. Therefore it can be inferred that there could exist some mathematical relation between D_2 and β. We thus found a surprisingly negative linear correlation between D_2 and β, where the correlation coefficient is 0.73 and the slope of fitting is ~1.86. This scaling behavior of the two complexity exponents, which also exists in many other critical physical systems, might agree with some previous findings claiming the evidence that brain may be working in the state of self-organized criticality (Gilden et al., 1995; Chen et al., 1997; Linkenkaer-Hansen et al., 2001).

We examined the EEG signals from different cortical layers and found a clear transition of the correlation dimension from a high to low across cortical layers in the primary somatosensory cortex. This result indicates that the corresponding EEG signals become successfully recruited into more synchronized activities with lower degrees of freedom from more chaotic states. It may be expected the similar spatio-temporal pattern of transition could be found in other primary sensory cortical areas that receive thalamic inputs. For those other cortical areas, such as in allocortex, showing heterogenous laminar structure that lack of direct thalamic inputs and layer IV, the distribution of the correlation dimension across the cortical layers would expect to be different from that in the present study.

Cortical neuronal networks consists of large assembles of neurons, their interactions with each other and their complex dynamic behavior may changes as the functional state of brain activity changed (Elbert et al., 1994). The changes in the D_2 of the EEG during different sleep stage and arousal states have been reported previously (Pijn et al. 1991; Achermann et al., 1994; Pradhan et al., 1995; Fell et al., 1996). In the present study, the averaged D_2 of each layer was uniformly decreased with increasing halothane concentrations. Similar effect of gas anesthesia on D_2 was found in a recent report (Widman et al., 2000). The neuronal activities were suppressed progressively with increase of anesthetic depth as evident by examining the evoked sink source patterns. However the tendency of layer dependency D_2 still remained. The maximal loss of complexity was found in the cortical layer 4 in higher anesthesia level. Thus it indicates that the intracortical D_2 is a sensitive measure to assess brain dynamics in different brain arousal states.

Different approaches, such as bispectral index, AAI^{TM} index and EEG entropy, have been developed to monitor the anesthetic depth in clinic. However there is still controversy regarding the predictive value for individual, response of linearity and inter-individual variation (Anderson et al., 2003; Anderson and Jakobsson, 2004; Rampil et al.; 1998, Muncaster et al., 2003). Although the aim in the present study did not attempt to provide a better solution of the monitoring the anesthetic depth

assessment, to be useful in clinical practice, more studies would need to perform such as computation of intra-cortical complexity in different brain regions and under different anesthetic agents, anesthetic dosage versus response profiles, non-invasive technique to detect the deep cortical potentials. Our finding did find out that intracortical activities may be a more sensitive index than the surface EEG to indicate the loss of consciousness.

Abbreviations

NTSA, nonlinear time series analysis method; D_2, correlation dimension; EEG, electroencephalogram; VPL, ventral posterior lateral; CSD, current source density; TISEAN, Nonlinear Time Series Analysis

Acknowledgements

Multichannel silicon probes were provided by the University of Michigan Center for Neural Communication Technology sponsored by NIH NIBIB grant P41-RR09754. This study was supported by grants from the National Science Council and the Academia Sinica, Taiwan, ROC.

References:

Achermann P, Hartmann R, Gunzinger A, Guggenbuhl W, Borbely AA. Correlation dimension of the human sleep electroencephalogram: cyclic changes in the course of the night. Eur J Neurosci 1994;6:497-500.

Anderson RE, Barr G, Assareh H, Jakobsson J. The AAI index, the BIS index and end-tidal concentration during wash in and wash out of sevoflurane. Anaesthesia 2003;58:531-5.

Anderson RE, Jakobsson JG. Entropy of EEG during anaesthetic induction: a comparative study with propofol or nitrous oxide as sole agent. Br J Anaesth 2004 ;92:167-70.

Anokhin AP, Birbaumer N, Lutzenberger W, Nikolaev A, Vogel F, Age increases brain complexity., Electroencephalography and Clinical Neurophysiology, 1996;99: 63-68.

Babloyantz A, Destexhe A. Low dimensional chaos in an instance of epileptic seizure. Proc Nat Acad Sci USA 1986;83:3513-7.

Babloyantz A, Salazar JM, Nicolls C. Evidence of chaotic dynamics of brain activity during the sleep cycle. Phys Lett A 1985;111:152 – 6.

Binzegger T, Douglas RJ, Martin KAC. Axons in Cat Visual Cortex are topologically self-similar. Cerebral cortex 2004; doi:10.1093/cercor/bhh118.

Chen Y, Ding M, Scott Kelso JA. Long Memory Processes (1/f alpha Type) in Human Coordination. Phys Rev Lett 1997;79:4501–4504.

Crick F, Koch C. Constraints on cortical and thalamic projections: the no-strong-loops hypothesis. Nature 1998;391:245–250.

Douglas RJ, Martin KA. Neuronal circuits of the neocortex. Annu Rev Neurosci 2004;27:419-51.

Egolf DA, Greenside HS. Relation between fractal dimension and spatial correlation length for extensive chaos. Nature 1994;369:129-131.

Elbert T, Ray WJ, Kowalik ZJ, Skinner JE, Graf KE, Birbaumer N. Chaos and physiology: deterministic chaos in excitable cell assemblies. Physiol Rev 1994;74:1-47.

Feldmeyer D, Lubke J, Silver RA, Sakmann B. Synaptic connections between layer 4 spiny neurone-layer 2/3 pyramidal cell pairs in juvenile rat barrel cortex: physiology and anatomy of interlaminar signalling within a cortical column. J Physiol. 2002;538:803-22.

Fell J, Roschke J, Mann K, Schaffner C. Discrimination of sleep stages: a comparison between spectral and nonlinear EEG measures. Electroencephalogr Clin Neurophysiol 1996;98:401-10.

Ferri R, Elia M, Musumeci SA, Stam CJ. Non-linear EEG analysis in children with

epilepsy and electrical status epilepticus during slow-wave sleep (ESES). Clinical Neurophysiology 2001;112:2274–80.

Freeman, JA, Nicholson C. Experimental Optimization of Currrent Source Density Technique for Anuran Cerebellum. J Neurophysiol 1975;38:369-82.

Gilden DL, Thornton T, Mallon MW.1/f noise in human cognition. Science. 1995;267:1837-9.

Glass L, Guevara MR, Shrier A. Universal bifurcations and the classification of cardiac arrthymias. Ann NY Acad Sci 1987;584:168-178.

Grassberger P. Nature. 1986;323: 609-612.

Grassberger P. Nature. 1987;326: 524.

Grassberger P. Procaccia I. Measuring the Strangeness of Strange Attractors. Physica D, 1983;9:189-208.

Hegger R, Kantz H, Schreiber T. Practical implementation of nonlinear time series methods: The TISEAN package, CHAOS 1999;9:413-35.

Jeong J, Kim SY, Han SH. Nonlinear Dynamical Analysis of the EEG in Alzheimer's Disease with Optimal Embedding Dimension. Electroencephalography and Clinical Neurophysiology, 1998;106: 220-8.

Jones EG. Microcolumns in the cerebral cortex. Proc Natl Acad Sci USA 2000;97: 5019–5021.

Kantz H, Schreiber T. Nonlinear Time Series Analysis. Cambridge University Press, 1997.

Kawaguchi Y, Kubota Y. GABAergic cell subtypes and their synaptic connections in rat frontal cortex. Cereb Cortex 1997;7:476-86.

Kotini A, Anninos P. Detection of non-linearity in schizophrenic patients using magnetoencephalography. Brain Topogr. 2002;15:107-13.

Lee Y-J, Zhu Y-S, Xu Y-H, Shen M-F, Zhang H-X, Thakor NV. Detection of non-linearity in the EEG of schizophrenic patients. Clinical Neurophysiology 2001;112:1288-1294.

Lehnertz K. Nonlinear Time Series Analysis of Intracranial EEG Recordings in Patients with Epilepsy- an overview. Int J Psychophysiol 1999;34:45-52.

Linkenkaer-Hansen K, Nikouline VV, Palva JM, Ilmoniemi RJ. Long-range temporal correlations and scaling behavior in human brain oscillations. J Neurosci. 2001; 21:1370-7.

Maffei A, Nelson SB, Turrigiano GG. Selective reconfiguration of layer 4 visual cortical circuitry by visual deprivation. Nat Neurosci 2004;7:1353-1359.

Martin KA. Microcircuits in visual cortex. Curr Opin Neurobiol. 2002;12:418-25.

Mitzdorf U. Current source-density method and application in cat cerebral cortex: investigation of evoked potentials and EEG phenomena. Physiol Rev

1985;65:37-100.

Mountcastle VB. The columnar organization of the neocortex. Brain 1997;120: 701–722.

Mountcastle VB. Introduction. Computation in cortical columns. Cereb Cortex 2003;13:2–4.

Muncaster AR, Sleigh JW, Williams M. Changes in consciousness, conceptual memory, and quantitative electroencephalographical measures during recovery from sevoflurane- and remifentanil-based anesthesia. Anesth Analg. 2003; 96:720-5.

Nicolis C and Nicolis G. Nature 1984a; 311: 529-532.

Nicolis C and Nicolis G. Nature 1984b; 326: 523.

Osborne A R and Provenzale A. Physica (Amsterdam) 1989; 35D: 357-381.

Pereda E, Gamundi A, Nicolau MC, Rial R, Gonzalez J. Interhemispheric differences in awake and sleep human EEG: a comparison between non-linear and spectral measures. Neurosci Lett 1999;263:37-40.

Peters A, Kara DA. The neuronal composition of area 17 of rat visual cortex. I. The pyramidal cells. J Comp Neurol 1985a;234:218-41.

Peters A, Kara DA. The neuronal composition of area 17 of rat visual cortex. II. The nonpyramidal cells. J Comp Neurol 1985b;234:242-63.

Peters A, Kara DA. The neuronal composition of area 17 of rat visual cortex. IV. The organization of pyramidal cells. J Comp Neurol 1987;260:573-90.

Pijn JP, Van Neerven J, Noest A, Lopes da Silva FH. Chaos or noise in EEG signals: dependence on state and brain site. Electroenceph clin Neurophysiol 1991;79:371-381.

Powell TPS, Mountcastle VB. Some aspects of the functional organization of the cortex of the postcentral gyrus of the monkey: a correlation of findings obtained in a single unit analysis with cytoarchitecture. Bull Johns Hopkins Hosp 1959; 105: 133–62.

Pradhan N, Sadasivan PK, Chatterji S, Dutt DN. Patterns of attractor dimensions of sleep EEG. Comput Biol Med 1995;25:455-462.

Rampil IJ, Kim JS, Lenhardt R, Negishi C, Sessler DI. Bispectral EEG index during nitrous oxide administration. Anesthesiology 1998;89:671-7.

Roschke J, Mann K, Fell J. Nonlinear EEG dynamics during sleep in depression and schizophrenia. Int J Neurosci 1994;75:271-84.

Scannell JW, Burns GA, Hilgetag CC, O'Neil MA, Young MP.The connectional organization of the cortico-thalamic system of the cat. Cereb Cortex. 1999; 9:277-99.

Schreiber T and Schmitz A. Phys. Rev. Letts., 1996; 77: 635-638.

Skoglund TS, Pascher 1R, Berthold CH. Aspects of the organization of neurons and dendritic bundles in primary somatosensory cortex of the rat. Neurosci Res 2004;50:189–198.

Stam CJ, Jelles B, Achtereekte HA, Rombouts SA, Slaets JP, Keunen RW. Investigation of EEG non-linearity in dementia and Parkinson's disease. Electroencephalogr Clin Neurophysiol. 1995;95:309-17.

Steriade M, Timofeev I. Neuronal Plasticity in Thalamocortical Networks during Sleep and Waking Oscillations. Neuron 2003;37:563–576.

Stoop R, Blank D, Kern A, v d Vyver JJ, Christen M, Lecchini S, Wagner C. Collective bursting in layer IV. Synchronization by small thalamic inputs and recurrent connections. Cogn Brain Res 2002;13:293-304.

Swanson L.W. Brain maps: Structure of the rat brain, Amsterdam: Elsevier Science Publishers, 1992.

Szentagothai J. The ‘‘module concept’’ in cerebral architecture. Brain Res 1975;95: 475–496.

Takens F. Detecting Strange Attractors in Turbulence. Lecture Notes in Math. Vol. 898, New York: Springer-Verlag, 1981.

Theiler J. Phys. Lett. A 1991; 155: 480-483.

Theiler J. On the evidence for low-dimensional chaos in an epileptic

electroencephalogram. Phys Lett A 1995;196: 335-341.

Turrigiano GG, Nelson SB. Homeostatic plasticity in the developing nervous system. Nat Rev Neurosci. 2004;5:97-107.

Van Cappellen van Walsum AM, Pijnenburg YA, Berendse HW, van Dijk BW, Knol DL, Scheltens P, Stam CJ. A neural complexity measure applied to MEG data in Alzheimer's disease. Clin Neurophysiol 2003;114:1034-40.

Van der Heyden MJ, Velis DN, Hoekstra BPT, Pijn JPM, van Emde Boas W, van Veelen CWM, van Rijen PC, Lopes da Silva FH, DeGoede J. Non-linear analysis of intracranial human EEG in temporal lobe epilepsy. Clin Neurophysiol 1999;110:1726-1740.

Widman G, Schreiber T, Rehberg B, Hoeft A, Elger CE. Quantification of depth of anesthesia by nonlinear time series analysis of brain electrical activity. Phys. Rev. E 2000;62:4898-4903.

Woolsey TA, van der Loos H,. The structural organization of layer IV in the somatosensory region (S1) of mouse cerebral cortex. Brain Res 1970;17: 205–242.

Table 1 Mean and standard deviation of D_2 of original data and corresponding surrogate data (n=9)

Channel no.	Original data	Surrogate data
1	2.85 ± 0.32	2.89 ± 0.33
2	2.94 ± 0.34	2.94 ± 0.31
3	3.04 ± 0.37	3.16 ± 0.43
4	3.33 ± 0.28	3.47 ± 0.34
5	3.48 ± 0.13	3.60 ± 0.19
6	3.18 ± 0.09	3.41 ± 0.10
7	3.07 ± 0.19	3.22 ± 0.18
8	2.91 ± 0.20	3.03 ± 0.18
9	2.84 ± 0.31	2.94 ± 0.27
10	2.78 ± 0.28	2.84 ± 0.27
11	2.68 ± 0.27	2.75 ± 0.21
12	2.56 ± 0.19	2.62 ± 0.20
13	2.59 ± 0.25	2.62 ± 0.22
14	2.59 ± 0.25	2.61 ± 0.20
15	2.65 ± 0.31	2.66 ± 0.30
16	2.73 ± 0.29	2.69 ± 0.25

Table 2

The D_2 and β in different cortical layer

	Layer I	Layer II/III	Layer IV	Layer V	Layer VI
D_2	2.67 ± 0.11*	2.79 ± 0.13*△	3.24 ± 0.03	2.79 ± 0.16*△	2.53 ± 0.12*
β	1.24 ± 0.03*	1.15 ± 0.05*◇	0.95± 0.05	1.14± 0.06*☆	1.30± 0.04*

***** $p<0.01$, compared with D_2 in layer IV

△ $P<0.05$, compared with D_2 in layer VI

◇ $P<0.05$, compared with D_2 in layer VI

☆ $p<0.01$, compared with D_2 in layer VI

Data were shown as mean ± s.e.m.(n=5).

Table 3

The percent changes of D_2, comparing with D_2 in 0.75%, in different cortical layers under 1% and 2% halothane concentrations

Cortical layers	D_2 (1%)/ D_2 (0.75%)	D_2 (2%)/ D_2 (0.75%)
I	0.981 ± 0.021	0.926 ± 0.042
II/III	1.007 ± 0.058	0.954 ± 0.091
IV	0.932 ± 0.019	0.753 ± 0.052
V	0.917 ± 0.031	0.759 ± 0.057
VI	0.949 ± 0.017	0.830 ± 0.061

Data were shown as mean ± s.e.m.(n=5).

Table 4

The ANOVA of correlation dimension of the intracortical EEG from different cortical layers and changes of halothane concentrations.

D_2	squares	d.f.	Mean square	F	p
Layers, within groups	0.147	4	0.037	4.712	0.0161
Halothane, within groups	0.101	1	0.101	3.105	0.176
Layers x halothane	0.034	4	0.008	11.697	0.0004

Table 5

The ANOVA of correlation dimension of the intracortical EEG from different cortical layers and treatment conditions.

D_2	squares	d.f.	Mean square	F	p
Layers, within groups	4.657	4	1.164	49.611	< 0.001
Conditions, within groups	0.235	2	0.118	5.014	0.012
Layers x halothane	0.258	8	0.032	1.374	0.238

Figure legends

Figure 1. The spontaneous EEG recordings in 16 channel (from cortical layer I to layer VI) of an 8 s epoch extracted from original 160 s records. The corresponding cortical layers were labeled in the right of the panel.

Figure 2. An example of multichannel recordings of evoked potentials and their CSD profiles. The field potentials showed evoked positive response in the superficial layer (I,II/III), but potentials reversed to negativity from layer IV. The CSD in layer IV exhibited earliest sink current after electrical stimulation. The downward direction of the current is the sink and the upward direction of the current is the source.

Figure 3. Correlation dimension and phase portrait in different channels or different cortical layers. (a) The averaged correlation dimension on each channel was obtained from 20 subsets, 8 s, in one rat. Data were shown mean and S.D.. (b) The time delay (t = 80 ms) phase portraits of channels representing different layers showed different geometric patterns. (c) The D_2 of each cortical layer averaged from 5 rats. The D_2 in layer IV exhibited the largest value.

Figure 4. Power spectrum and scaling exponent in different channels or cortical layers. (a-e) The Fast Fourier Transform power spectrums of channels representing different cortical layers. (f) In the log-log scale, the power spectrum density showed the power law character as demonstrated in one channel in cortical layer VI. (g) The

power spectrum densities of low frequency (square), alpha (triangle), beta (circle), and gamma (diamond) bands exhibited the cortical layer dependence. (h) The cortical layer dependence of scaling exponent. The power density decreasing in low frequency band but increasing in other bands (shown in Figure3.b) in layer IV made the fractal exponent small.

Figure 5. The scaling exponent versus averaged correlation dimension plot of 5 rats demonstrated a negative correlation between each other.

Figure 6. The effect of different the halothane concentrations on the evoked responses and the correlation dimension. (a) The amplitudes of the evoked CSD profiles in different halothane concentration. (b) Effect of halothane on intacortical D_2 in 16 channels in one example. (c) Effect of the changes of halothane, 0.75% to 1% and 0.75% to 2%, on the D_2 in different cortical layers.

Figure 7. Reversible deactivation of thalamic activities and the effect of blocking thalamic input drives on the cortical layer complexity. (a) Schematic diagram of the placement of recording-microinjection hybrid electrode, Michigan probe and the anatomical location of thalamic nuclei. The solid lines delineated the approximate diffusion range of the solution injected into the VPL thalamic nucleus in 4 different animals. The blackened areas was the converging the overlapped areas. Note that the Michigan probe and hybrid electrode were not placed in the same coronal plane in

actual experimental setting. (b) Evoked response before, during and 30 min after the microinjection of I μl of lidocaine. A typical example of evoked thalamic and cortical CSD profile following the peripheral electrical stimulation was shown. The evoked thalamic unit activities were shown in the upper sweeps. Noted that the thalamic unit responses were completely abolished and the sink currents across the layers were markedly reduced after the injection. Both of the effect were recovered almost completely 30 min after. (c) D_2 data were calculated and collected from spontaneous EEG signals before, during and 30 min after the injection of lidocaine in four different animals. D_2 values from histologically verified cortical layers were pooled. D_2 in layer IV was significantly decreased after the injection whereas D_2 in other layers did not show significant change. No difference of D_2 in different cortical layers 30 min after injection compared with that before injection was found.

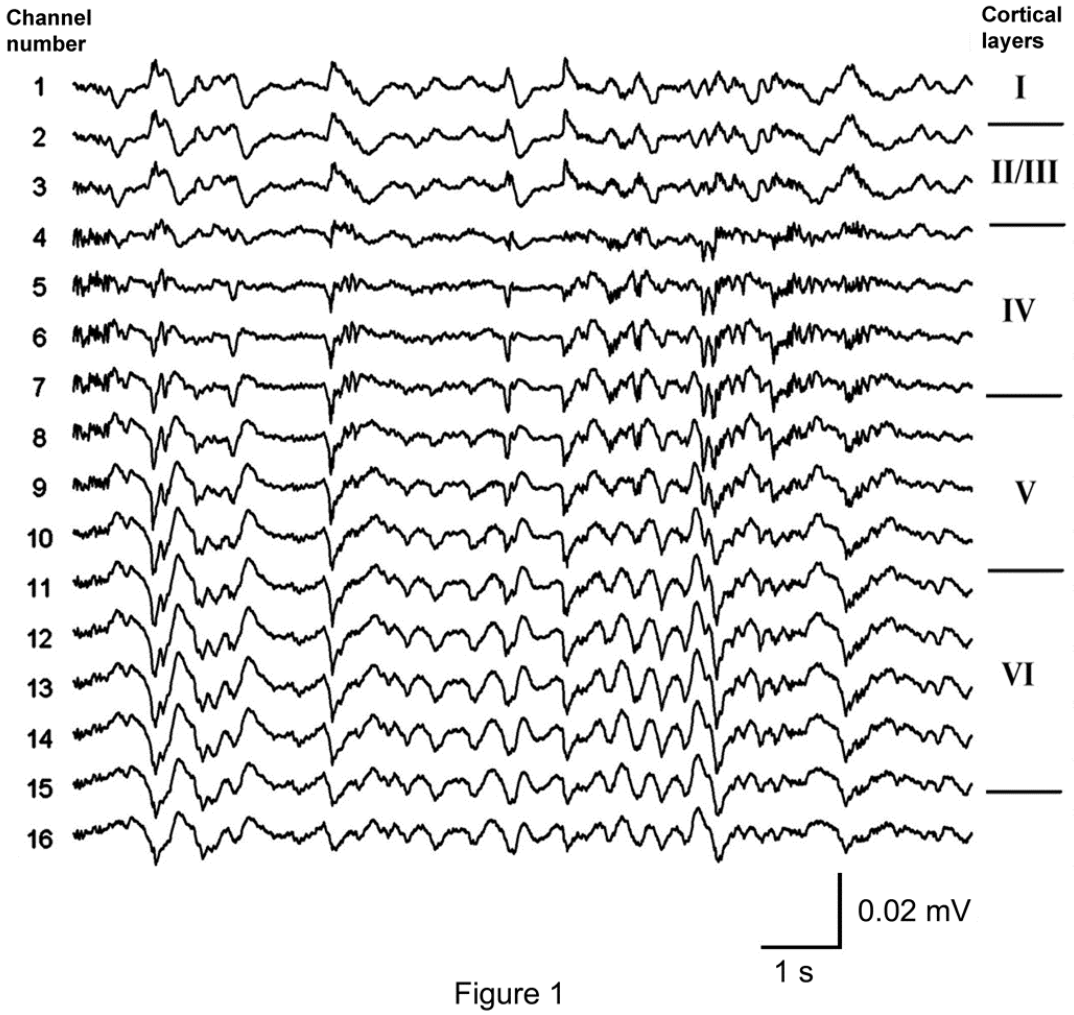
Channel number
Cortical layers
1
2
3
4
5
6
7
8
9
10
11
12
13
14
15
16
I
II/III
IV
V
VI
0.02 mV
1 s

Figure 1

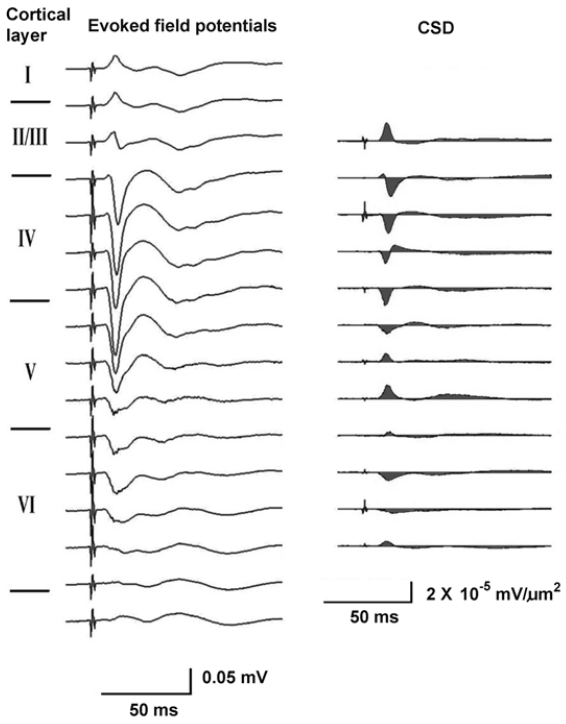
Cortical layer
Evoked field potentials
CSD
I
II/III
IV
V
VI
0.05 mV
50 ms
2 X 10-5 mV/μm2
50 ms

Figure 2

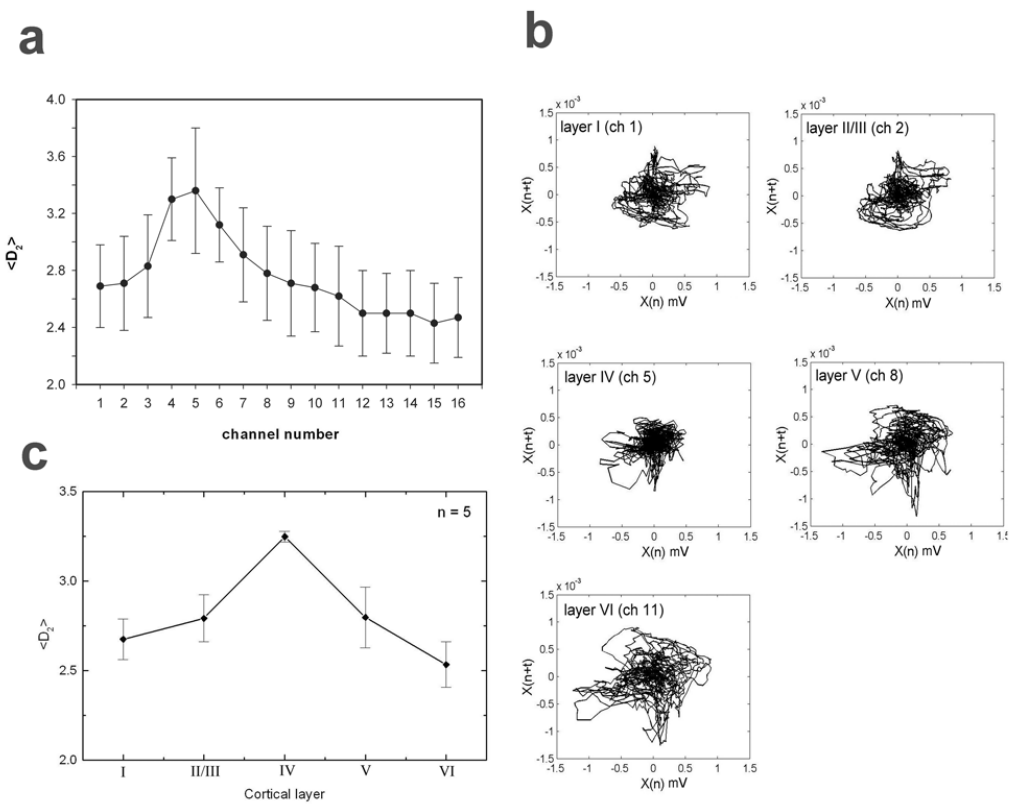
a
b
c
<D2>
channel number
Cortical layer
n = 5
I
II/III
IV
V
VI
layer I (ch 1)
layer II/III (ch 2)
layer IV (ch 5)
layer V (ch 8)
layer VI (ch 11)
X(n+t)
X(n) mV
x 10-3

Figure 3

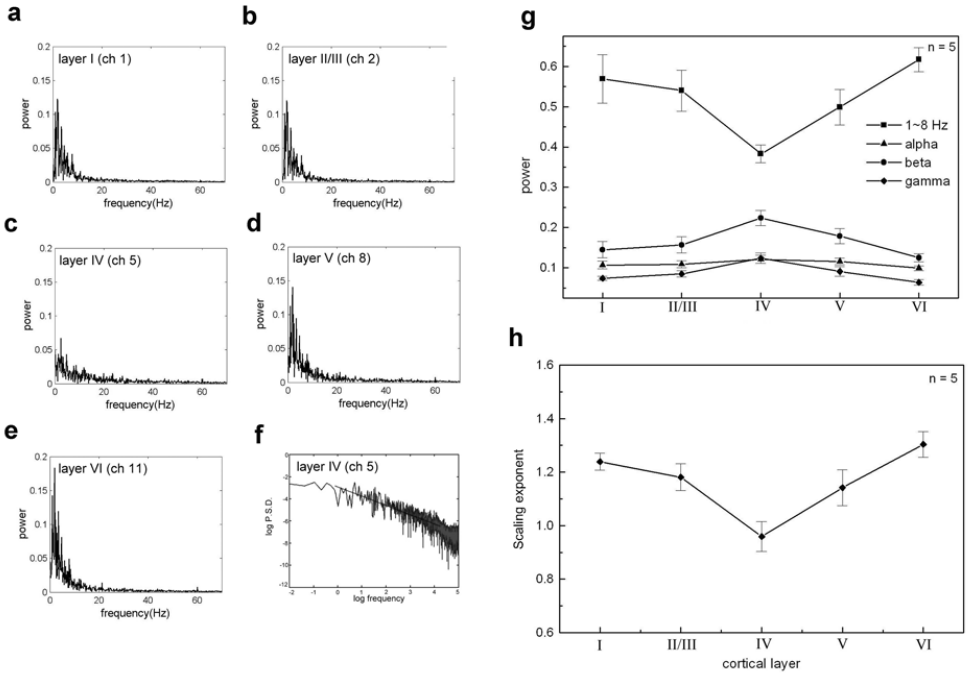
a
layer I (ch 1)
b
layer II/III (ch 2)
c
layer IV (ch 5)
d
layer V (ch 8)
e
layer VI (ch 11)
f
layer IV (ch 5)
power
frequency(Hz)
log P.S.D.
log frequency
g
n = 5
1~8 Hz
alpha
beta
gamma
power
I
II/III
IV
V
VI
h
n = 5
Scaling exponent
cortical layer

Figure 4

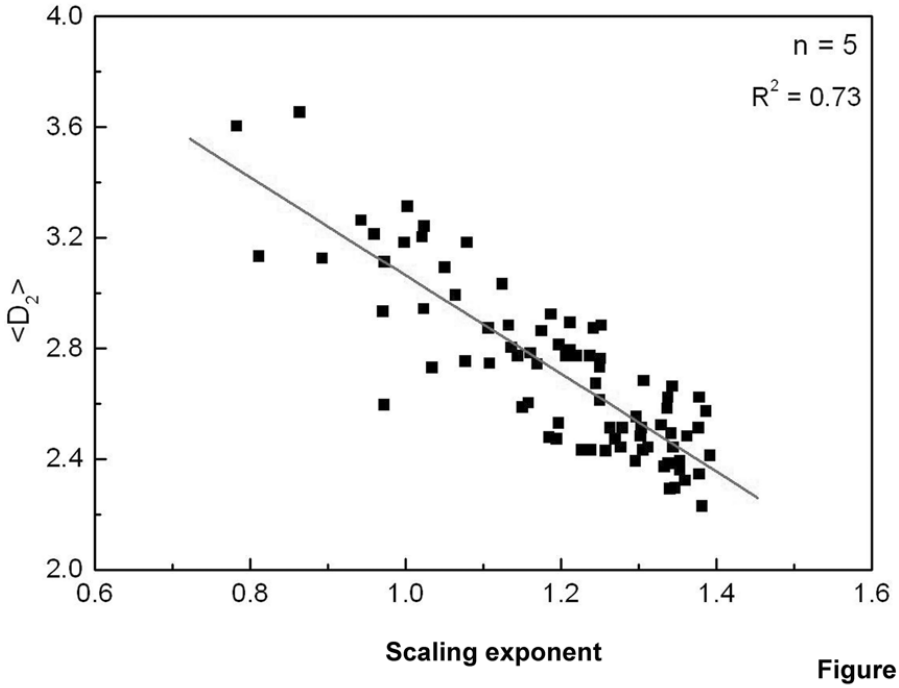

Figure 5

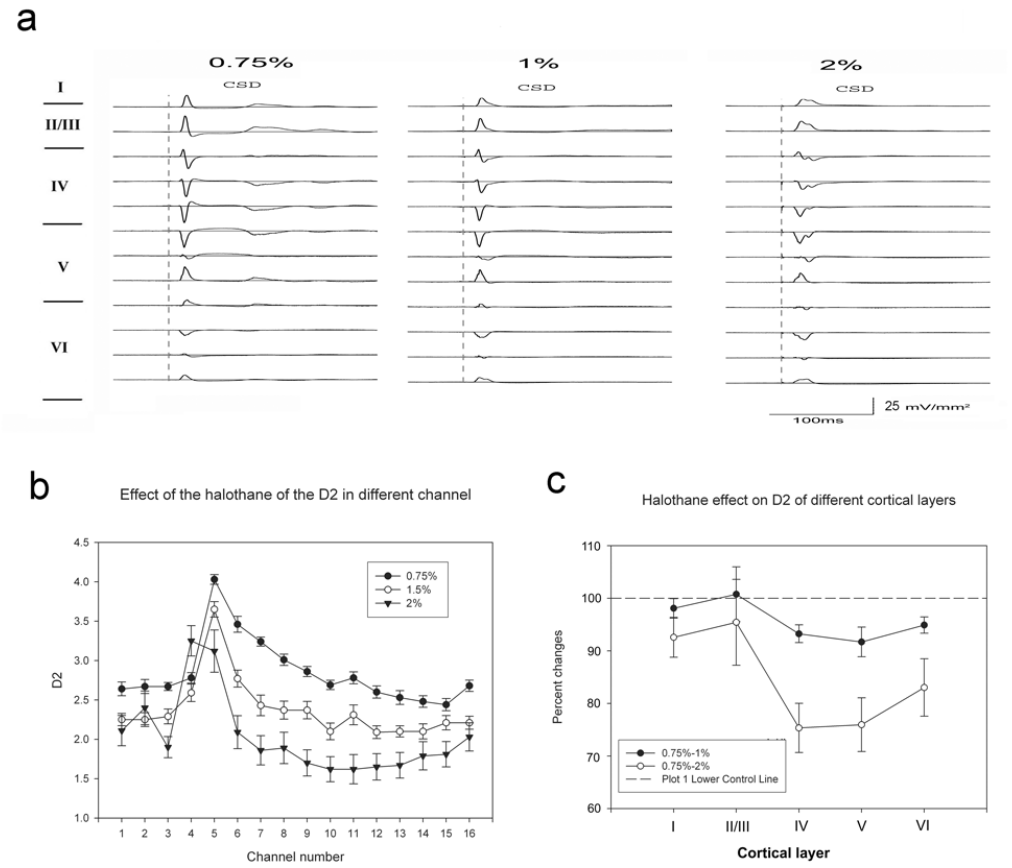
a
0.75%
1%
2%
CSD
I
II/III
IV
V
VI
25 mV/mm²
100ms
b
Effect of the halothane of the D2 in different channel
0.75%
1.5%
2%
D2
Channel number
c
Halothane effect on D2 of different cortical layers
Percent changes
0.75%-1%
0.75%-2%
Plot 1 Lower Control Line
Cortical layer

Figure 6

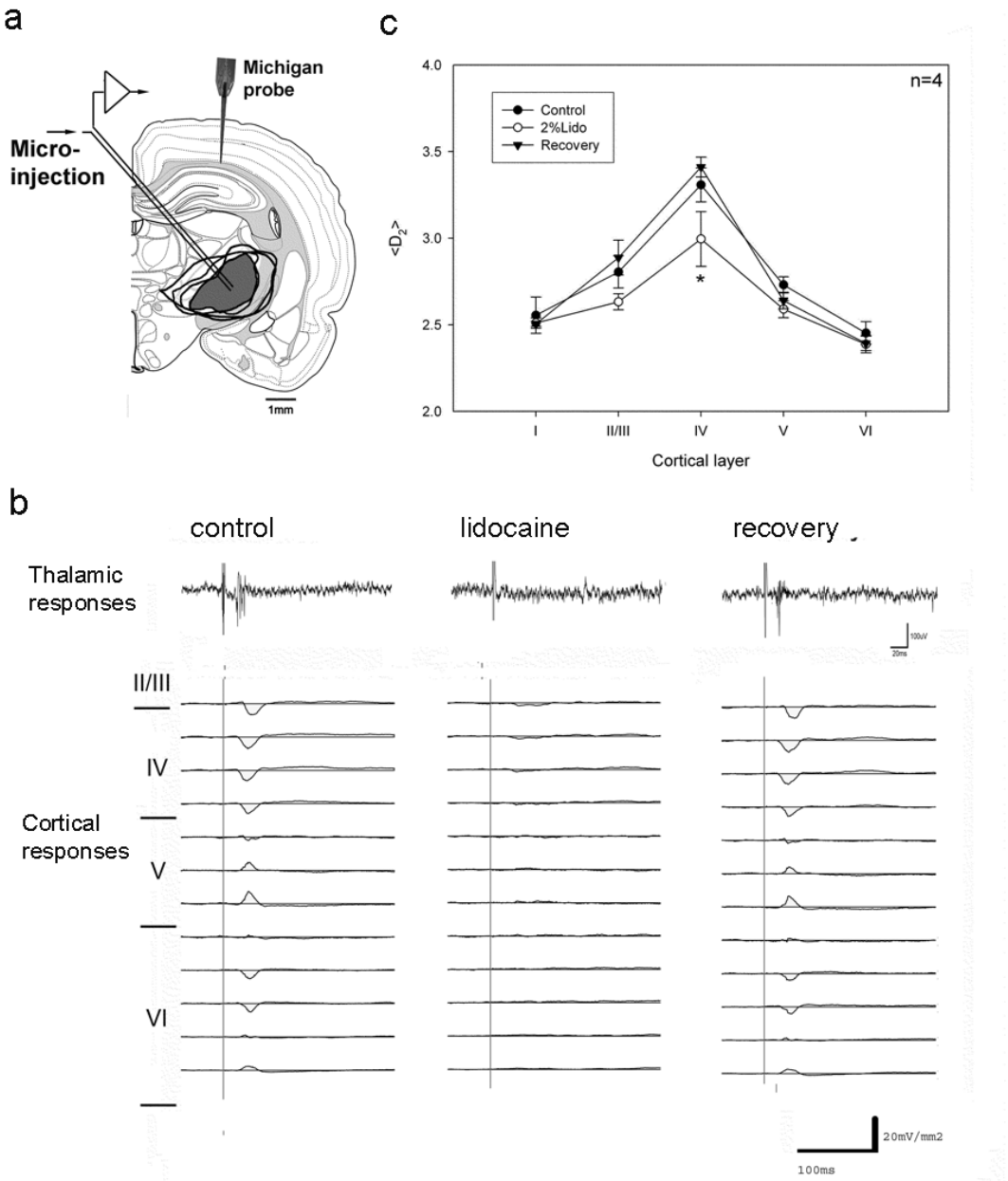
a
Michigan probe
Micro-injection
1mm
c
n=4
Control
2%Lido
Recovery
<D2>
4.0
3.5
3.0
2.5
2.0
I
II/III
IV
V
VI
Cortical layer
b
control
lidocaine
recovery
Thalamic responses
Cortical responses
II/III
IV
V
VI
20mV/mm2
100ms

Figure 7